Charge control and mobility studies for an AlGaN/GaN high electron mobility transistor

Yifei Zhang
Applied Physics Program, The University of Michigan at Ann Arbor, Ann Arbor, Michigan 48109-1120

Jasprit Singh
Department of Electrical Engineering and Computer Science, The University of Michigan at Ann Arbor, Ann Arbor, Michigan 48109-2122

(Received 25 June 1998; accepted for publication 21 September 1998)

A charge control model and a mobility model are developed for the Al–GaN/GaN high electron mobility transistor (HEMT) device. The model addresses issues of how piezoelectric effect and interface roughness influence device properties. We find that even small amount of interface roughness has very strong effect on the two-dimensional electron gas properties. Low-lying electronic states are strongly localized and transport through these states is not described by Born approximation but by phonon-assisted hopping. At low temperature the effects of localization are quite important and we use the Kubo formula to study this transport. Results for charge control and mobility are presented as a function of Al composition in the AlGaN/GaN HEMT. © *1999 American Institute of Physics.* [S0021-8979(99)01101-9]

I. INTRODUCTION

Group III-nitride semiconductors have attracted wide attention recently in view of their application in high power devices and optoelectronic devices with wavelengths ranging from the red into the ultraviolet. These materials have direct bandgaps from 1.9 eV for InN through 3.4 eV for GaN to 6.2 eV for AlN. Tremendous efforts have been devoted to the optoelectronic devices based on GaN and the related ternary alloys. For example, the blue and violet laser emission at room temperature in InGaN/GaN/AlGaN-based heterostructures under pulsed currents and continuous-wave operation[1–8] has been demonstrated. Furthermore, blue- and green-light-emitting diodes with GaInN quantum wells have already been commercialized.[9] In the application of high power devices such as microwave electronic devices, the performance of the devices depends on the quality of heterostructure interface formed by the materials with different bandgaps as well as the quality of the materials grown.

There are two important issues that govern the AlGaN/GaN high electron mobility transistors (HEMTs) which are significantly different from HEMTs made from structures such as AlGaAs/GaAs or InAlAs/InGaAs. The first has to do with the very strong piezoelectric effect present due to the lattice mismatch between AlGaN and GaN. It is known that group III nitrides have large piezoelectric constants along the (0001) direction.[10–13] When (0001)-oriented thin AlGaN layers are grown psuedomorphically on a thick GaN, the biaxial strain induces a piezoelectric field in the material. As a result, there is a strong interface charge at the HEMT interface. The second effect has to do with interface roughness. Although this effect is present in other HEMT structures as well, the larger band discontinuity combined with larger effective mass in the channel makes interface roughness much more important in controlling the channel mobility. Additionally, the combination of interface roughness and piezoelectric effect can cause the charges at the interface to be distributed nonuniformly.

We have developed a numerical formula to study the charge control and transport of AlGaN/GaN-based HEMT device. The charge control model is based on a self-consistent solution of the Poisson equation and Schrödinger equation. Piezoelectric effect due to strain is modeled by including a polarization field.

In examining transport in the two-dimensional channel, we note that much of our understanding of transport in semiconductor devices depends upon the use of Born approximation and the independence of various scattering mechanisms. Scattering mechanisms such as ionized impurity scattering, interface roughness scattering, alloy scattering, etc. are handled within the Born approximation and are assumed to act independently. In many problems of interest, it is known that Born approximation is not valid but it is still used because of the complexity of the problem. Examples include transport in metal–oxide–semiconductor field effect transistors (MOSFETs) at low temperature when a significant fraction of carriers are in the localized bandtail states, transport in clustered alloys etc. For the AlGaN/GaN system, our simulations show that there is considerable localization of low lying electronic states. Born approximation becomes invalid under these conditions. We use the Kubo formula to study transport under such conditions. The breakdown of Born approximation reflects itself in mobility increasing with temperature—a signature of hopping conductivity. At high temperatures, the Kubo formula and Born approximation give similar results. The temperature at which the two formalisms become equally valid depends on the interface roughness parameters. In this article we explore some of these issues.

In the next section, we provide details of the formalism for charge control and mobility. In Sec. III we present our

results. We also discuss the comparison of these results with experimental results for charge control and mobility. Conclusions are presented in Sec. IV.

II. FORMALISM

To study charge control and channel mobility we need to examine in detail the band profile and scattering theory in a HEMT. As noted in the introduction, in the AlGaN/GaN HEMT, interface roughness and piezoelectric effects are expected to play a dominant role. We develop our model in two steps—the first one designed to address the charge control picture and the second to see the influence of interface roughness on transport.

A. Charge control model

Our model first obtains the potential profile in a HEMT structure by solving the Schrödinger equation and Poisson equation self-consistently. The Schrödinger equation yields the confined charge terms in the Poisson equation which, in turn, determines the potential profile. This potential profile is fed back into the Schrödinger equation until the solution of Poisson equation goes to convergence.

For the charge control description, the AlGaN/GaN interface is treated as an ideal interface with abrupt transition from channel material, GaN to barrier material, AlGaN. Due to the large piezoelectric constants of group III nitrides, the piezoelectric effect plays an important role in determining the performance of the AlGaN/GaN-based HEMT device. The piezoelectric effect is taken into account by applying the boundary condition for the AlGaN/GaN interface in the first step,

$$\epsilon_1 \mathbf{E}_1 + \mathbf{P}_1 = \epsilon_2 \mathbf{E}_2 . \tag{1}$$

Where ϵ_1 and ϵ_2 are the dielectric constants and $\mathbf{E}_1$ and $\mathbf{E}_2$ are electric fields at the interface of AlGaN and GaN, respectively. Quantity $\mathbf{P}_1$ is the polarization (piezoelectric field) caused by the in-plane tensile strain in AlGaN. The magnitude of the polarization vector is given by[17]

$$P_1 = 2d_{31}(c_{11} + c_{12} - 2c_{13}^2/c_{33})\mu_{xx}, \tag{2}$$

where strain tensor component, u_{xx}, is

$$u_{xx} = \mu_{yy} = \frac{a_2 - a_1}{a_1} \tag{3}$$

for a pseudomorphically grown AlGaN with the growth direction along (0001) direction. Here d_{31} is the relevant piezoelectric constant, c_{ij} are the elastic coefficient, and a_1 and a_2 are the lattice constants for AlGaN and GaN, respectively. We use the value of the polarization field,[13] 6.0×10^6 V/cm for AlN grown on GaN. The polarization field in $Al_xGa_{1-x}N$ is evaluated by multiplying this value by the Al fraction, x in the barrier.

The direction of the piezoelectric field depends on the face orientation. For AlGaN/GaN heterostructures grown on sapphire, the GaN surface at the heterointerface can be either nitrogen or gallium terminated.[14,15] In order to determine the direction of the piezoelectric field in the strained AlGaN layer, it is usually assumed that in GaN, as in other III–V semiconductors, the in-plane tensile strain induces electric field pointing from a cation-terminated interface to an anion-terminated interface (i.e., from a gallium interface to a nitrogen interface).[16,17] Therefore, in gallium-terminated strained heterostructures, the piezoelectric effect reduces the two-dimensional electron density. On the contrary, in the nitrogen-terminated strained heterostructures the piezoelectric effect enhances the two-dimensional electron density. Thus these heterostructures should be the choice for the HEMT devices. In our study, we assume nitrogen-terminated strained heterostructures.

The one-dimensional Poisson equation can be written as

$$\frac{d^2}{dz^2} E_c(z) = -\frac{\rho(z)}{\epsilon(z)}, \tag{4}$$

where E_c is the conduction band profile in the device, ρ is the total charge density, and ϵ is the dielectric constant which can be changed in different regions of the device to account for different material parameters across interfaces. The total charge density ρ is the sum of the doping charge, the free charge including the hole and electron, and the quantum-confined charge. This can be written as

$$\rho(z) = q\left(N_d^*(z) - N_a^*(z) - n_{\text{free}}(z) + p_{\text{free}}(z) - \sum_i n_i \psi_i^*(z)\psi_i(z) \right), \tag{5}$$

where N_a^* and N_d^* are the effective doping concentrations, n_{free} and p_{free} are the free carrier concentrations, and the sum is over i two-dimensionally confined subbands of which normalized envelope functions are ψ_i and in which the occupation is n_i (p_i for the hole case). The effective doping concentrations, N_d^* and N_a^* can be written as

$$N_d^* = N_d\left(\frac{1}{1 + 2e^{(E_f - E_d)/k_B T}} \right), \tag{6}$$

$$N_a^* = N_a\left(\frac{1}{1 + 4e^{(E_a - E_f)/k_B T}} \right), \tag{7}$$

where N_d and N_a are the concentrations of donor and acceptor dopants, and E_d and E_a are the impurity ionization energies, respectively. The solution of the Poisson equation is performed by a vectorized Newton's method.

In the calculation of the charge density, one must determine the quantized two-dimensional charge and the free carrier charge. The quantized two-dimensional charge can be calculated from the eigen energy levels obtained by solving the Schrödinger equation. The free carrier charge density can be written as,

$$n_{\text{free}}(z) = N_c F_{1/2}\left(\frac{E_f - E_c(z)}{k_B T} \right), \tag{8}$$

where N_c is the material effective density of states and $F_{1/2}$ is a half-order Fermi integral. The reason we use Fermi–Dirac statistics instead of Boltzmann statistics, which have been used by many authors in the past, to determine the free carrier concentrations is that in heavily doped cases, the bands are near degenerate or degenerate, and Boltzmann sta-

tistics will overestimate the free carrier concentrations. To calculate the Fermi integral fast and accurately, a look-up table is used. Note that in Eq. (8), we use a three-dimensional effective density of states to obtain the free carrier charge. However, to distinguish two-dimensional carriers from three-dimensional ones in the quantum well region, a cut-off value, which usually is set to be the lower boundary value, is used. For those carriers whose energy is below this cut-off value, they are treated as two-dimensional gas. For those whose energy is above this cut-off value, they are thus treated as free carriers. In order to determine the two-dimensionally confined charge profile, one must solve the Schrödinger equation for the subband envelope functions and their occupations. The z-dependent part of the Schrödinger equation is strictly separable from the in-plane part of the equation which gives us extended Bloch-like states. The one-dimensional (z dependent) Schrödinger equation can be written using the perpendicular part of the effective mass tensor as follows:

$$\frac{d^2}{dz^2}\,\psi_n(z)+\frac{2m_w}{\hbar^2}\,[E_n-V(z)]\psi_n(z)=0, \tag{9}$$

where m_w represents electron effective mass along the quantum confinement direction.

Once the Schrödinger equation has been solved for the envelope functions and the subband energy levels, it is straightforward to calculate the subband occupations. Since the subband density of states is constant with energy, the occupation comes from the first-order Fermi integral which is analytically integrable. In the electron case, we can write the occupation as

$$n_i=\frac{m_i k_B T}{\pi\hbar^2}\,\ln\left[1+\exp\left(\frac{E_i-E_f}{k_B T}\right)\right], \tag{10}$$

where m_i is the in-plane effective mass.

B. Model for mobility

In most calculations for transport in HEMTs, Born approximation is used to calculate scattering rates from various scattering sources. These sources are treated as independent mechanisms and their combined effect is calculated by using the Mathieson's rule for mobility. Interface roughness scattering is treated in the same spirit in these calculations. The interface region is described as the region containing random fluctuations of islands with a certain island height and lateral extent. Using island height and lateral extent as fitting parameters, reasonably good agreement with experiments at room temperature[18] has been demonstrated in high quality MOSFETs and HEMTs.

The use of Born approximation and independent scattering mechanism model is valid if the scattering potential is weak and does not cause localization of states. We will see in the result section that in the case of the AlGaN/GaN devices the interface roughness effects are quite strong and cause electronic wave function localization. Under these conditions Born approximation becomes invalid. To calculate the electron transport properties such as conductivity and mobility in cases where there are localized states the Kubo formula[19] has been used. It is important to note that results obtained through the Kubo formula reduce to those obtained by Born approximation when the perturbation is weak.

To find the conductivity and mobility within Kubo formula it is necessary to solve the eigenstates of the problem *in presence of the perturbation*. This of course makes the problem numerically very intensive. To apply Kubo formula, it is necessary to solve for a three-dimensional Hamiltonian including the interface roughness. Availability of high speed computers has now allowed us to solve the three-dimensional HEMT problem in a reasonable amount of time.

After the one-dimensional potential is obtained from the first step, it is fed into the three-dimensional Schrödinger equation to yield the electronic spectrum with or without the presence of the interface roughness. The three-dimensional Schrödinger equation for the envelope functions is given by

$$\left[-\frac{\hbar^2}{2m_i}\,\nabla^2+V(x,y,z)\right]\psi(x,y,z)=E\,\psi(x,y,z), \tag{11}$$

where $V(x,y,z)$ is a three-dimensional potential incorporated with the interface roughness.

The rough interface is composed of islands of either the barrier region (AlGaN) or the channel region (GaN). These islands are randomly placed on the interface by a Monte Carlo method. To keep the model simple, when the island is of AlGaN composition, the potential is set to be the potential value of the barrier, whereas when the island is of GaN, the potential is set to be the potential value of the channel. The three-dimensional Schrödinger equation is solved by the finite-difference technique. The boundary conditions along xy plane (parallel to the interface) are chosen to be periodic in order to calculate the transport quantities. The typical size of matrix involved in our calculation is in the order of $10^4\times10^4$. Since we solve for the electronic levels in the presence of the interface roughness in the HEMT channel, the effect of this roughness on the microscopic and macroscopic properties of the structure can be calculated directly from the electronic spectrum. The Kubo formula for the conductivity of electron under a small dc field is given by

$$\sigma=\frac{2\pi e^2\hbar^3 V}{m^{*2}}\int-\frac{\partial f}{\partial E}\,|D(E)|^2N^2(E)dE, \tag{12}$$

where the reduced momentum matrix element, $D(E,E')$ is expressed as

$$D(E,E')=\int_{E=E'}\psi_E\,\frac{\partial}{\partial x}\,\psi_{E'}dr. \tag{13}$$

Equation (12) will render a conductance rather than conductivity. Once the conductance is derived, the mobility is readily calculated by the relation,

$$\mu=\frac{\sigma}{ne}, \tag{14}$$

where n is the sheet charge density in the channel and e is the electron charge.

To include the influence of other scattering mechanisms like phonon scattering, we need to calculate the eigenstates of the HEMT in presence of phonons. Within the adiabatic

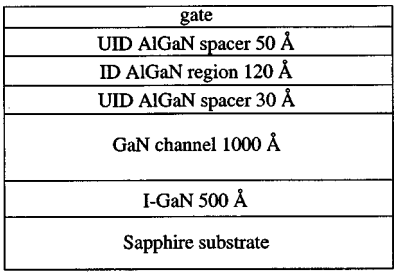

FIG. 1. Structure of the HEMT device in our study.

approximation, the phonons can be considered to cause a broadening of the energy levels. We calculate this broadening within the Born approximation. A Gaussian broadening function is used for both the density of states, $N(E)$ and the reduced momentum matrix, $D(E)$. The reduced momentum matrix is evaluated by

$$|D|^2_{\mathrm{av}}=\frac{\Sigma_i|\int \psi_{E_i}\frac{\partial}{\partial x}\psi_E d^3x|^2 w_\Gamma(E_i,E)}{\Sigma_i w_\Gamma(E_i,E)}, \tag{15}$$

where $w_\Gamma(E_i,E)$ is an integral over the overlapping region between two Gaussian broadening functions centering on energy levels, E_i and E, respectively. The quantity Γ is the width of the broadening functions and represents the lifetime of the corresponding state due to the effects of scatterings (phonons). Several groups have used the Kubo formula[20–22] for studying transport at 0 K. In these studies the conductivity is calculated at the limit of Γ going to zero. To extend the Kubo formalism to finite temperature, we use a phenomenological relation between scattering processes arising due to finite temperature and Γ. This is similar in spirit to the approach taken in deriving Mott variable range conductivity. This approach allows us to examine how phonon scattering and interface roughness scattering influence transport without treating them as independent scattering mechanisms. In this approach we view the total Hamiltonian as

$$H=H_{\mathrm{interface}}+H^*_{\mathrm{phonon}}, \tag{16}$$

where $H_{\mathrm{interface}}$ is the Hamiltonian for the problem where interface roughness effects are included and result in localized eigenstates. The effect of H^*_{phonon} is to cause a width to these eigenstates due to the vibration of the lattice. We evaluate this width by calculating the acoustic phonon scattering rates.[23]

In our model as temperature increases, two effects occur: (i) the carrier distribution spreads out due to the broadening of the Fermi function; (ii) the broadening of the individual eigenvalues occurs due to the increased phonon scattering. The outcome is that just as in Mott variable range conductivity mobility increases with temperature initially. This is because electrons localized at some region in space can now couple with more states. As the temperature increases to high values we expect that phonon scattering will eventually suppress mobility. It is important to note that in Kubo formula, the electronic spectrum is obtained by solving the full Hamiltonian with the presence of interface roughness so that any correlation caused by the interface roughness is automatically included in the electronic spectrum.

TABLE I. Material parameters for the charge control model.

	Symbol	Unit	GaN value	AlN value
Energy gap	E_g	eV	3.4	6.2
Donor ionization energy	E_d	meV	25	25
Dielectric constant	ϵ	ϵ_0	10.0	8.5
Electron effective mass	m_e	m_0	0.2	0.48
Hole effective mass	m_h	m_0	0.6	0.6

III. RESULTS

The structure of the HEMT device in our study is shown in Fig. 1. The *n*-type barrier, AlGaN is unintentionally and intentionally doped (UID and ID) at 1×10^{18} and 3×10^{18} cm^{-3}, respectively. The channel region is lightly doped at 4×10^{16} cm^{-3}. The material parameters used are given in Table I. Since the hole effective mass for AlN is not available, it is set to be the same as that of GaN. Material parameters for the alloy are not well documented in the literature over the wide range of composition used in our study. In the absence of such data, alloy material parameters are obtained by linear interpolation of the GaN and AlN values. The Schottky barrier is taken to be 1.2 eV and the conduction band discontinuity is assumed to be 75% of the bandgap discontinuity.

A typical result obtained from our model for *n*-type HEMTs is shown in Fig. 2. The simulation is done for 300 K device operation. The figure shows the conduction band profiles in a $Al_{0.15}Ga_{0.85}N$/GaN HEMT device with and without the piezoelectric effect. As can be seen from the figure, the piezoelectric effect is the main source of two-dimensional electron charge in the device. Without the piezoelectric effect (a relaxed layer case), the device is actually depleted near the AlGaN/GaN interface. Simulations for the low temperature show similar result. It is clear that the piezoelectric

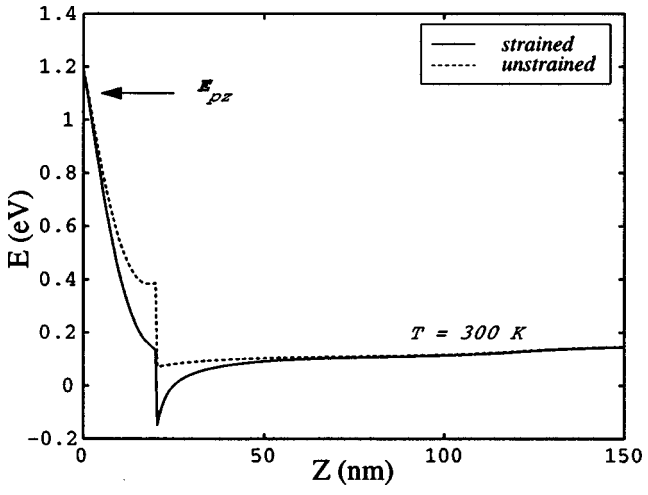

FIG. 2. Conduction band profiles at 300 K for the (a) strained (solid line) and (b) unstrained (dotted line) barrier, $Al_{0.15}Ga_{0.85}N$. The piezoelectric field E_{pz} in the barrier is in the growth direction.

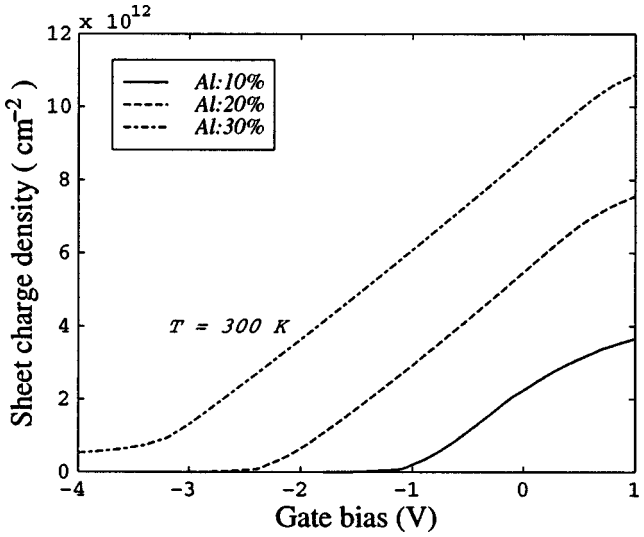

FIG. 3. Sheet charge density vs gate bias for different Al contents at 300 K.

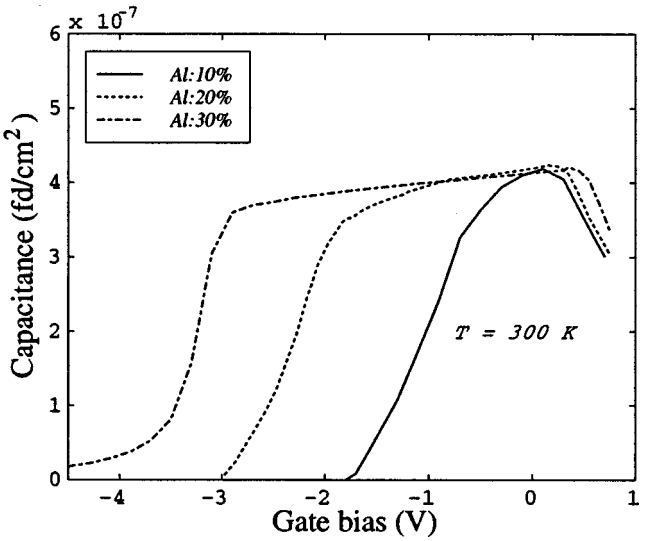

FIG. 4. Capacitance vs gate bias for different Al contents at 300 K.

field plays a critical role in the HEMT and is the primary source of electron charge in the device.

The Al content in the AlGaN layer alters the strain (if the layer is pseudomorphically grown) and the conduction band discontinuity between the barrier and the channel. Increasing Al content will increase the strain in the layer and thus increase the piezoelectric field. Combined with the increasing conduction band discontinuity, the two-dimensional electron charge will increase. However, as we show later as the Al content increases, the interface roughness effects become more serious. We see that as the sheet charge density increases, the electrons are pushed more closely to the interface and thus are more easily affected by the interface roughness and piezoelectric charge at the interface. This leads to large scattering rate due the interface roughness and the piezoelectric charge. Also the device becomes more difficult to turn off. This is primarily due to the large piezoelectric field present in the AlGaN layer and large conduction discontinuity. From a growth point of view it becomes more difficult to grow the barrier psuedomorphically on the GaN. The high Al content barrier layer may relax through dislocations resulting in the degradation of the device performance. Therefore, there has to be an optimization in the Al content.

In Fig. 3 we show the sheet charge density as a function of gate bias. HEMT devices with three different Al content barriers are simulated at 300 K. As shown in the figure, when the Al content increases in the barrier, the threshold voltage of the device becomes more negative. The threshold voltages for barriers with 10%, 20%, and 30% Al, are -3.6, -2.4 and -1.2 V, respectively. However, in the active region of the device operation, the sheet charge densities show linear relations with the gate bias and have the same slopes which indicate the same capacitance–voltage relation over the active region. The capacitance–voltage relations are shown in Fig. 4. The peaks of the capacitance curves correspond to the active regions of the devices and are independent of the Al content.

Our next step is to study the consequences of interface roughness and piezoelectric effect on transport of the HEMT device. To understand how sheet charge and Al composition influence interface roughness scattering, we examine the nature of the free carrier profile in the 2D channel. In Fig. 5 we show the quantum-confined charge density profiles in the device at zero gate bias. We see that as the Al composition increases, the electron density increases and is shifted closer to the interface. This is clarified further in Figs. 6 and 7.

In Fig. 6 we show the fractional charge within 5 and 10 Å of the interface region for Al composition of 20% as a function of sheet charge density. In Fig. 7 the fraction near the interface is shown as a function of Al composition at zero gate bias. We can see that interface roughness effects will be quite serious as Al composition increases.

Interface roughness is introduced by randomly placing islands on the intermixed region of the HEMT structure with island size given by

$$\Delta L_x = 25 \text{ Å}; \quad \Delta L_y = 25 \text{ Å}; \quad \Delta L_z = 5,10 \text{ Å}. \tag{17}$$

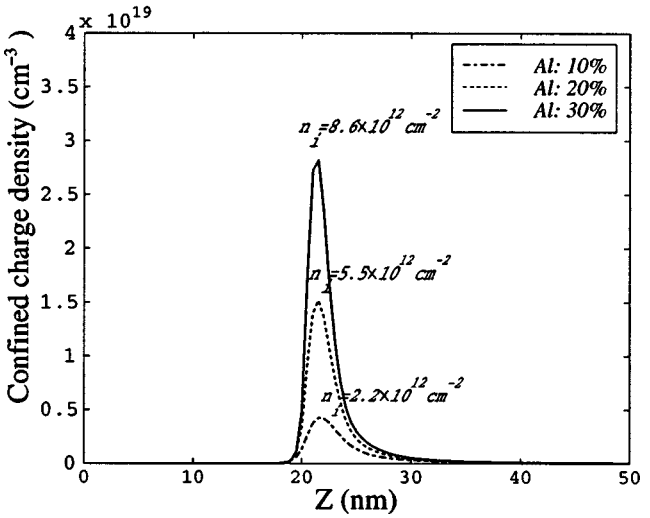

FIG. 5. Quantum-confined charge density profiles in the device for different Al contents at 300 K.

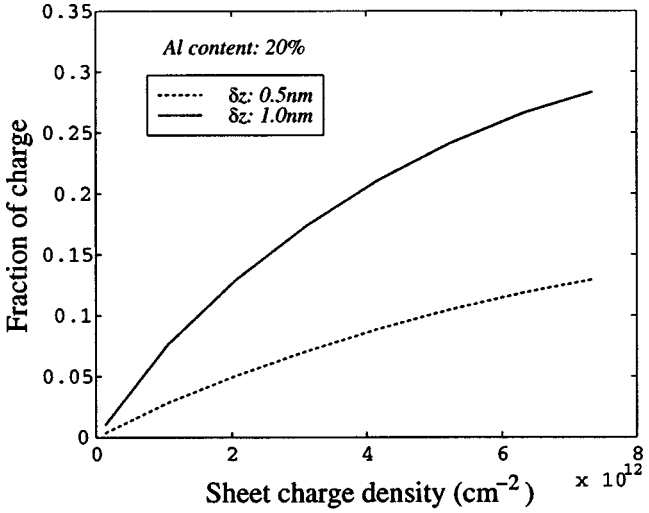

FIG. 6. Fraction of charge vs sheet charge density within 5, and 10 Å of the interface region for Al composition of 20%.

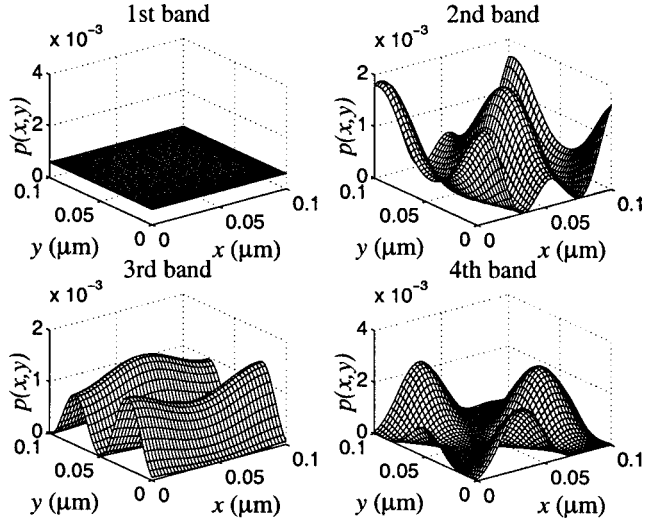

FIG. 8. Electron probability distribution functions $P(x,y)$ for a perfect interface. The wave functions extend to the device (chosen to be 0.1 μm×0.1 μm).

In Figs. 8 and 9 we show the electron probability distribution functions $P(x,y)$ on xy plane in a HEMT with a perfect interface and a rough interface, respectively. The Al content in the barrier is 20%. The gate is biased at 0 V corresponding to a sheet charge density of 5.2×10^{12} cm^{-2}. The operating temperature is assumed to be 77 K. From Fig. 8, one can see that the electron wave functions for a perfect interface extend over the entire device and have a peak amplitude of 0.0020 corresponding to the normalization in the 1000×1000 Å xy plane. However, for the imperfect interface the eigenstates are quite different. We see from Fig. 9 that the low-lying states are strongly localized e.g., the peak amplitude of the first state is 0.015, one order of magnitude larger than the case for the perfect interface). The lateral spread of these state is 200–250 Å. The position of these low-lying states will change if we change the random sequence of the disorder but the localization length is in the same range. This suggests that to study transport in such a system the use of the Born approximation is invalid. We also see that as we go to higher energy states, the states become extended and are spread over the entire structure.

The results for the density of states are shown in Fig. 10. We focus on the density of states near the band edges since these states are most influenced by interface roughness. The height of random islands at the interface, ΔL_z, are chosen to be 5 and 10 Å. The density of states is calculated by using a 2 meV Gaussian broadening function. As can be seen from Fig. 10, when there is a high sheet charge density in the channel, the density of states is significantly affected by the interface roughness and bandtails are seen to develop as the interface roughness increases. This strong localization in the low-lying states can be attributed to the strong quantum confinement along the z direction. This strong z confinement leads to a large fraction of electrons occupying the interfacial region.

Next, we report results for the mobility in the channel using Kubo formula. From our discussion of localization, we can see that for the imperfect interface, mobility will be very small unless electrons can couple from one state to another by other scattering processes such as phonons. Thus for the imperfect interface case, we expect that as the broadening parameter Γ increases, mobility will initially increase. For the case of the perfect interface, on the other hand, as Γ increases the mobility should decrease.

For the HEMT at 77 K, acoustic phonon scattering is expected to be the dominant scattering mechanism. Phonon scattering actually assists the conduction in the inversion layer for the device with interface roughness at low Γ value which results in an increase in the mobility at small Γ. This is observed in the experiment and becomes a signature of varying range hopping conductivity. Using the acoustic phonon scattering rates for the GaN channel we find that Γ is expected to be 0.39 meV.

In Fig. 11 we show the calculated relationship between the mobility and Al composition. The results are shown for two different interface island sizes. Also shown are the re-

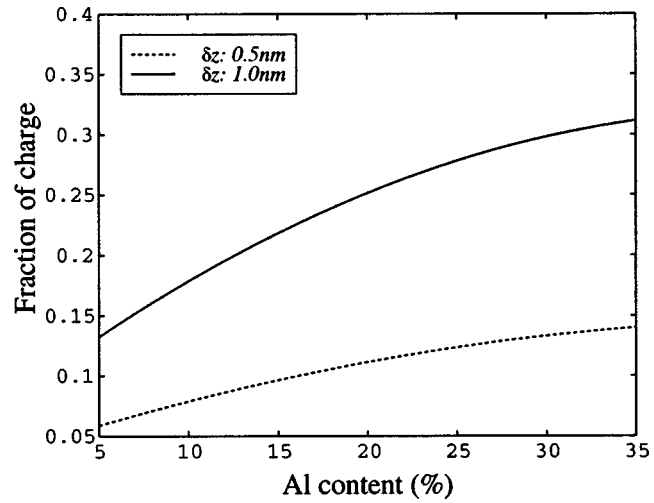

FIG. 7. Fraction of charge vs Al content within 5 and 10 Å of the interface region.

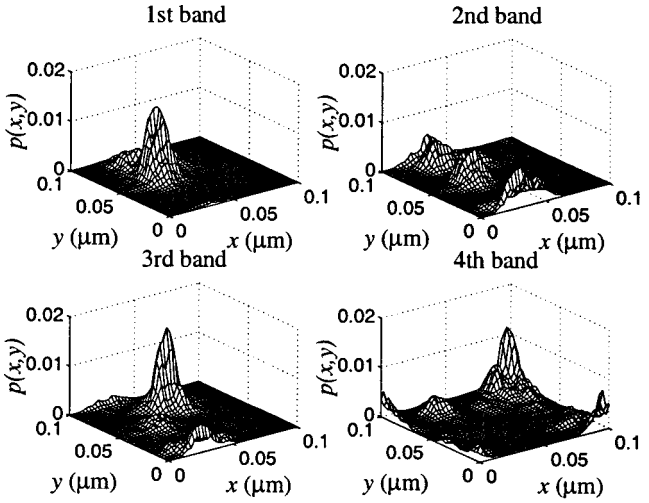

(a) Localized states

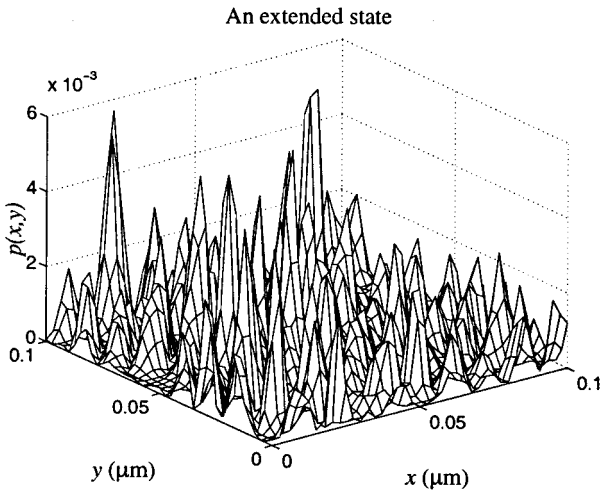

(b) Extended state

FIG. 9. Electron probability distribution functions $P(x,y)$ with an interface roughness (height: 5 Å, lateral extension: 25 Å). The low-lying states are clearly localized but the excited states are extended.

sults for a perfect interface. We see that for the perfect interface there is no degradation of mobility with increased Al composition in the barrier. However, in presence of interface roughness we see that as the Al composition increases the mobility in the channel degrades. This is in agreement with experimental results which also show a similar degradation.[24]

In Fig. 12 we show the mobility as a function of temperature. As can be seen from the figure that the mobility for small Al content (10%) decreases with temperature in the range of study but for large Al content, the mobility initially increases due to the phonon-assisted scattering and then decreases. For comparison, we have also shown results for a perfect interface.

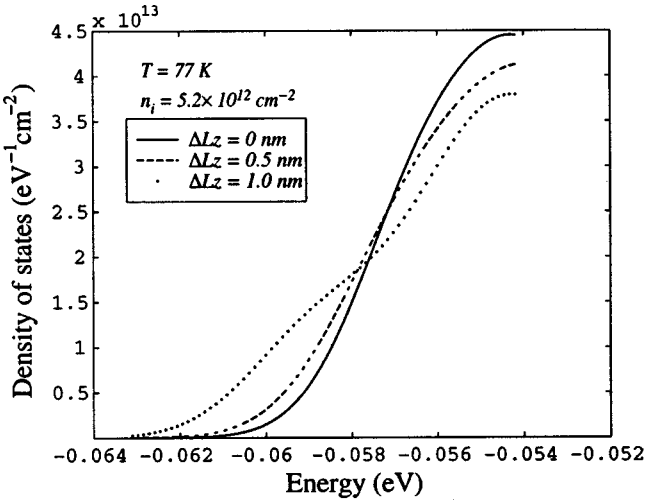

FIG. 10. Density of states functions with different interface roughness. The interface roughness causes significant bandtail states, especially for $\Delta L_z = 1.0$ nm.

IV. CONCLUSIONS

In this article, we have presented a charge control model for the AlGaN/GaN HEMTs. The effect of strain and piezoelectric effect on the charge in the two-dimensional channel has been included. We find that a very high sheet charge density can be produced due to the strong piezoelectric effect at the interface. The sheet charge density increases with increase in Al fraction in the barrier. The increase is primarily due to the higher piezoelectric charge.

We have also solved the three-dimensional Schrödinger equation for the HEMT in presence of interface roughness. We find that even a small amount of interface roughness causes localization of low lying electron levels. To study transport in such a system, we have used the Kubo formula. Our results show that for strong interface roughness the mobility around 77 K is essentially independent of temperature and even shows a region where it increases with temperature.

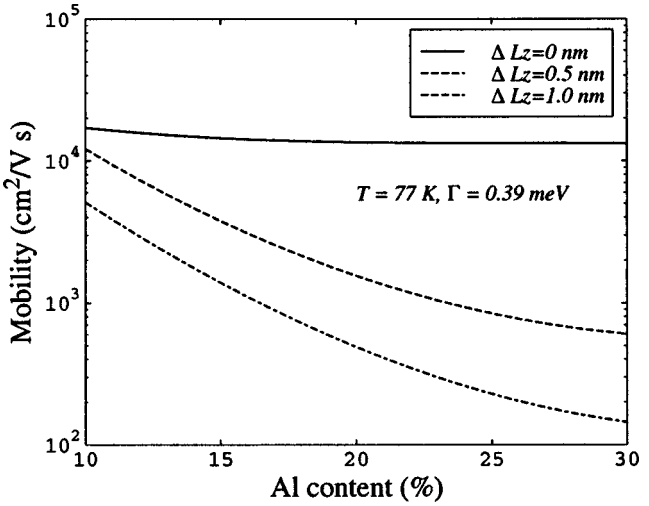

FIG. 11. Electron mobility as a function of Al content with different interface roughness.

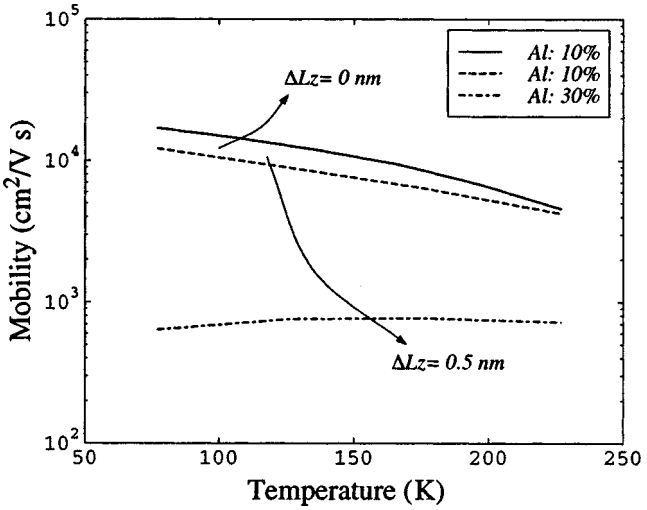

FIG. 12. Electron mobility as a function of temperature with different Al contents. Also shown is the electron mobility for a perfect interface.

The mobility in a HEMT with a rough interface degrades with increased Al composition in the barrier.

ACKNOWLEDGMENTS

The authors would like to thank Dr. U. Mishra's research group at UCSB for helpful feedback on this work. This work was funded by a grant from the Office of Naval Research.

[1] I. Akasaki, H. Amano, S. Nagahama, T. Tanaka, and M. Kaike, Jpn. J. Appl. Phys., Part 2 **34**, L1517 (1995).
[2] S. Nakamura, M. Senoh, S. Nagahama, N. Iwasa, T. Yamada, T. Matsushita, H. Kiyoku, and Y. Sugimoto, Jpn. J. Appl. Phys., Part 2 **35**, L74 (1996).
[3] S. Nakamura, M. Senoh, S. Nagahama, N. Iwasa, T. Yamada, T. Matsushita, H. Kiyoku, and Y. Sugimoto, Appl. Phys. Lett. **68**, 3269 (1996).
[4] S. Nakamura, M. Senoh, S. Nagahama, N. Iwasa, T. Yamada, T. Matsushita, Y. Sugimoto, and H. Kiyoku, Appl. Phys. Lett. **69**, 3034 (1996).
[5] K. Itaya *et al.*, Jpn. J. Appl. Phys., Part 2 **35**, L1315 (1996).
[6] G. E. Bulman *et al.*, Electron. Lett. **33**, 1556 (1997).
[7] M. P. Mack, A. Abare, M. Aizcorbe, P. Kozodoy, S. Keller, U. K. Mishra, L. Coldren, and S. DenBaars, MRS Internet J. Nitride Semicond. Res. **2**, 41 (1997).
[8] A. Kuramata, K. Domen, R. Soejima, K. Horino, S. Kubota, and T. Tanahashi, Jpn. J. Appl. Phys., Part 2 **36**, L1130 (1997).
[9] S. Nakamura, M. Senoh, N. Iwasa, S. Nagahama, T. Yamada, and T. Mukai, Jpn. J. Appl. Phys., Part 2 **34**, L1332 (1995).
[10] J. G. Gualtieri, A. Koshinski, and A. Ballato, IEEE Trans. Ultrason. Ferroelectr. Freq. Control **41**, 53 (1994).
[11] A. D. Bykhovski, B. Gelmont, M. S. Shur, and M. A. Khan, J. Appl. Phys. **77**, 1616 (1995).
[12] A. D. Bykhovski, V. V. Kaminski, M. S. Shur, Q. C. Chen, and M. A. Khan, Appl. Phys. Lett. **68**, 818 (1996).
[13] G. Martin, A. Botchkarev, A. Rockett, and H. Morkoc, Appl. Phys. Lett. **68**, 2541 (1996).
[14] R. Gaska, J. W. Yang, A. D. Bykhovski, M. S. Shur, V. V. Kaminski, and S. M. Soloviov, Appl. Phys. Lett. **71**, 3817 (1997).
[15] F. A. Ponce, D. P. Bour, W. T. Young, M. Saunders, and J. W. Steeds, Appl. Phys. Lett. **69**, 337 (1996).
[16] R. Gaska, J. W. Yang, A. D. Bykhovski, M. S. Shur, V. V. Kaminski, and S. M. Soloviov, Appl. Phys. Lett. **72**, 64 (1998).
[17] A. Bykhovski, B. Gelmont, and M. S. Shur, J. Appl. Phys. **74**, 6734 (1993).
[18] S. Yamakan, H. Ueno, K. Taniguchi, and C. Hamaguchi, J. Appl. Phys. **79**, 911 (1996).
[19] See, for example, S. Doniach and E. H. Sondheimer, *Green's Functions for Solid State Physicists* (W. A. Benjamin, Reading, MA, 1974).
[20] J. Stein and U. Krey, Z. Phys. B **37**, 13 (1980).
[21] D. J. Thouless and S. Kirkpatrick, J. Phys. C **14**, 235 (1981).
[22] S. Yoshino, in *Anderson Localization*, edited by Y. Nagaoka and H. Fukuyama (Springer, Berlin, 1982), p. 68.
[23] J. Singh, *Physics of Semiconductors and Their Heterostructures* (McGraw–Hill, New York, 1993).
[24] Y. Wu, Ph. D. dissertation, University of California at Santa Barbara, July 1997.